Mechanism and site of action of big dynorphin on ASIC1a

Borg, C.B.[1#], Braun, N.[1#], Heusser, S.A.[1], Bay, Y.[1], Weis, D.[1], Galleano, I.[1], Lund, C.[1], Tian, W.[2], Haugaard-Kedström, L.M.[1], Bennett, E.P.[2], Lynagh, T.[1], Strømgaard, K.[1], Andersen, J.[3], Pless, S.A.[1*]

[1]Department of Drug Design and Pharmacology, University of Copenhagen, Jagtvej 160, 2100 Copenhagen, Denmark

[2]Copenhagen Center for Glycomics, Departments of Cellular and Molecular Medicine and Odontology, University of Copenhagen, Blegdamsvej 3B, 2200 Copenhagen, Denmark

[3]Vipergen ApS, Gammel Kongevej 23A, 1610 Copenhagen, Denmark

[#] These authors contributed equally

* Correspondence:

Stephan A. Pless (stephan.pless@sund.ku.dk)

Center for Biopharmaceuticals, Department of Drug Design and Pharmacology

University of Copenhagen, Jagtvej 160, 2100 Copenhagen, Denmark

Abstract

Acid-sensing ion channels (ASICs) are proton-gated cation channels that contribute to synaptic plasticity, as well as initiation of pain and neuronal death following ischemic stroke. As such, there is a great interest in understanding the *in vivo* regulation of ASICs, especially by endogenous neuropeptides that potently modulate ASICs. The most potent endogenous ASIC modulator known to date is the opioid neuropeptide big dynorphin (BigDyn). BigDyn is upregulated in chronic pain and increases ASIC-mediated neuronal death during acidosis. Understanding the mechanism and site of action of BigDyn on ASICs could thus enable the rational design of compounds potentially useful in the treatment of pain and ischemic stroke. To this end, we employ a combination of electrophysiology, voltage-clamp fluorometry, synthetic BigDyn analogs and non-canonical amino acid-mediated photocrosslinking. We demonstrate that BigDyn binding induces ASIC1a conformational changes that are different from those induced by protonation and likely represent a distinct closed state. Using alanine-substituted BigDyn analogs, we find that the BigDyn modulation of ASIC1a is mediated through electrostatic interactions of basic amino acids in the BigDyn N-terminus. Furthermore, neutralizing acidic amino acids in the ASIC1a extracellular domain reduces BigDyn effects, suggesting a binding site at the acidic pocket. This is confirmed by photocrosslinking using the non-canonical amino acid azido-phenylalanine. Overall, our data define the mechanism of how BigDyn modulates ASIC1a, identify the acidic pocket as the binding site for BigDyn and thus highlight this cavity as an important site for the development of ASIC-targeting therapeutics.

Introduction

Neuropeptides are a diverse class of signalling molecules that are involved in a wide variety of physiological functions, including the modulation of neurotransmission (1, 2). The neuropeptide subclass of dynorphins is best known for its modulation of the G protein-coupled opioid receptors (3-5), through which they mediate spinal analgesia. However, it is increasingly recognised that these highly basic peptides also modulate the activity of ionotropic receptors, such as tetrameric glutamate receptors (N-methyl-D-aspartate (NMDA) subtype) and trimeric acid-sensing ion channels (ASICs) (6-10). The latter interaction is of particular interest, as ASICs have emerged as mediators of both pain and stroke and thus represent potential targets in the treatment of these diseases (11-17). In fact, big dynorphin (BigDyn) is the most potent endogenous ASIC modulator described to date. The neuropeptide was found to rescue proton-gated currents after exposure to steady-state desensitization (SSD)-inducing conditions in homomeric ASIC1a and heteromeric ASIC1a/2a and ASIC1a/2b channels in the nanomolar range and thereby promote acidosis-induced neuronal cell death in cultured neurons (10, 18). As ASIC1a homomers and ASIC1a-containing heteromers are the most prevalent isoforms in the nervous system, this raises the possibility that inhibitors or competitors of the ASIC1a-BigDyn interaction might prove valuable therapeutics. However, despite this potential therapeutic relevance, the underlying mechanism behind this potent modulation remains elusive.

BigDyn (32 aa) and two smaller peptides, dynorphin A (DynA, 17 aa) and dynorphin B (DynB, 13 aa), are tissue-specific cleavage products of the prodynorphin precursor peptide. DynA is evolutionarily highly conserved among mammals and amphibians and displays, along with BigDyn, high affinity for opioid receptors (4). BigDyn was reported to be ~1000-fold more potent in its modulation of ASIC1a SSD compared to DynA, while DynB did not modulate ASIC1a SSD (10). This raises the possibility of a unique ASIC-selective pharmacophore.

Here, we set out to investigate the molecular determinants of the high potency modulation of ASIC1a by BigDyn and identify the binding site on ASIC1a. Using a combination of

electrophysiology and voltage-clamp fluorometry we demonstrate that BigDyn reduces the proton sensitivity of both activation and SSD, likely by inducing a closed resting conformation of ASIC1a that is distinct from that induced by protons and psalmotoxin-1 (PcTx1). A collection of synthetic BigDyn analogs was generated and used to identify three positively charged amino acid residues at the N-terminus of BigDyn to be primarily responsible for the modulatory effects on ASIC1a. This is complemented by charge-neutralizing amino acid substitutions in the ASIC1a extracellular domain that identify negatively charged amino acids in the acidic pocket as the binding site for BigDyn. The location of the binding site is confirmed by incorporating the non-canonical amino acid photocrosslinker azido-phenylalanine (AzF) (19, 20) in the acidic pocket of ASIC1a to covalently crosslink ASIC-BigDyn complexes using UV exposure.

Results

BigDyn affects pH dependence of mASIC1a and induces a unique closed state

First, we set out to test the ability of BigDyn and its proteolytic products (Figure 1A) to rescue proton-gated currents after exposure to SSD-inducing conditions of wild-type (WT) mouse ASIC1a (mASIC1a) using two-electrode voltage clamp (TEVC) electrophysiology. SSD was induced using conditioning in pH 7.1, which decreased subsequent pH 5.6-induced current response to 5.7 % (95 % confidence interval (95CI): 3.8, 7.6 %) compared to that after conditioning in pH 7.4 ("control"). However, application of 1 μM BigDyn during the pH 7.1 conditioning step largely rescued pH 5.6-induced currents, resulting in 90.1 % (95CI: 77.9, 102.3 %) of the control current response. The EC_{50} for this current rescue was 210.6 nM (95CI: 162.6, 258.6 nM) BigDyn; Figure S1A-B). By contrast, applying DynA and DynB during conditioning did not produce significant current rescue when applied at a concentration of 1 μM (at pH 7.1) (Figure 1B-C), although at a concentration of 3 μM, DynA partially rescued pH 5.6-induced current (Figure S1C). Furthermore, co-application of 1 μM DynA or Dyn1-19 (containing the Arg18 and Lys19 that link DynA and DynB in full-length BigDyn) with DynB during conditioning did not reproduce the phenotype observed with full-length BigDyn (Figure 1B-C). Next, we sought to assess if the presence of BigDyn would affect the pH dependence of activation or SSD in WT mASIC1a. Indeed, even the presence of a sub-saturating BigDyn concentration (100 nM) resulted in a significant right-shift in the pH_{50} activation (from 6.80 (95CI: 6.70, 6.91) to 6.66 (95CI: 6.61, 6.70) in presence of 0.1 μM BigDyn, $p = 0.0172$) and SSD (from 7.21 (95CI: 7.19, 7.24) to 7.15 (95CI: 7.12, 7.19), $p = 0.0225$) (Figure 1D, Table S1).

The above results suggested that the potency of both proton activation and SSD was lowered in the presence of BigDyn, but it remained unclear if this occurred through a stabilization of the canonical resting closed state (relative to open/steady-state desensitized states) or if BigDyn induced a distinct protein conformation. To distinguish between these

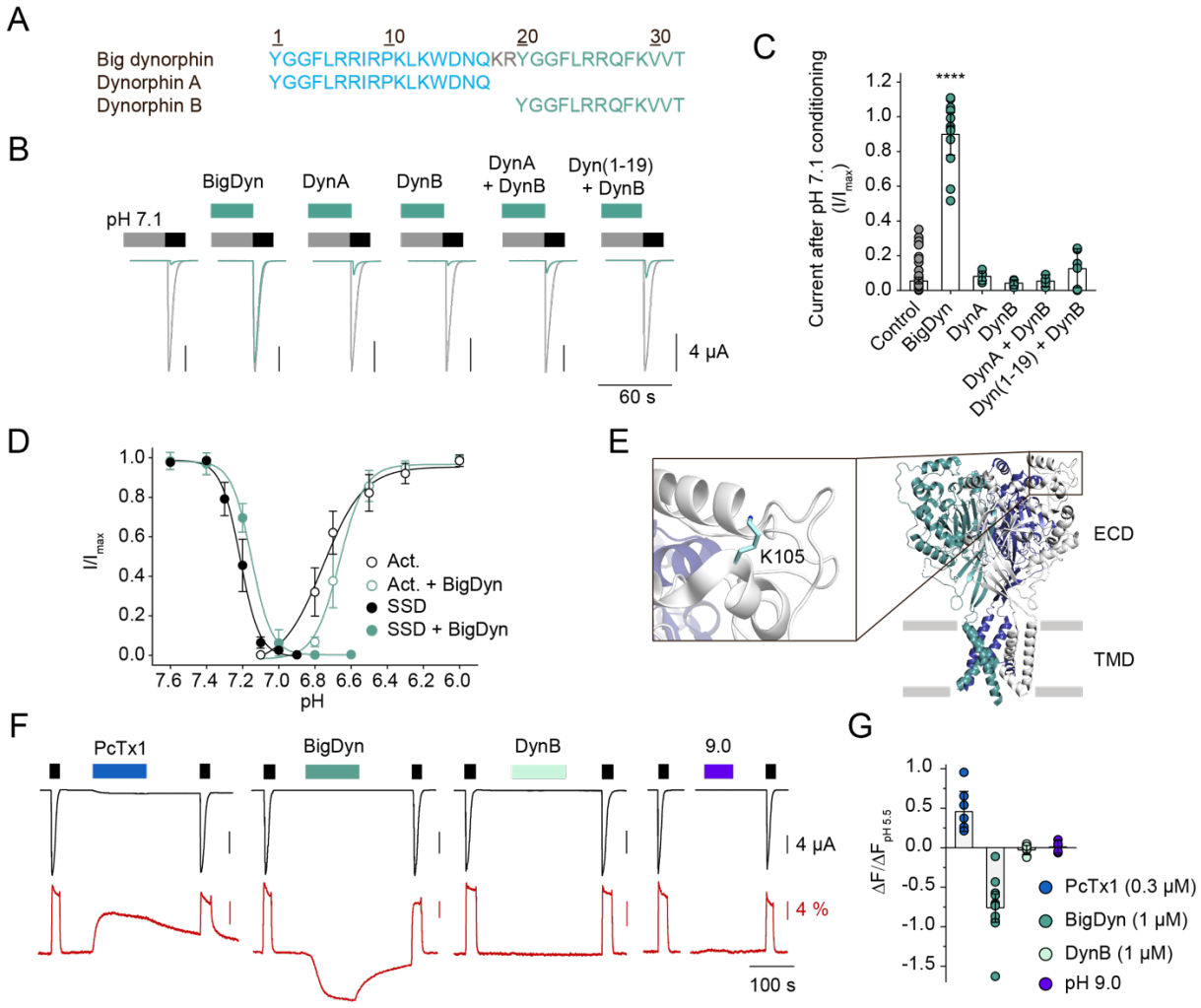

Figure 1: Mechanism of ASIC1a modulation by BigDyn. (A) Amino acid sequences of BigDyn, DynA and DynB. (B/C) Representative current traces (B) and averaged data (C) obtained by pH 5.6 application (black bar in (B)) at mASIC1a WT-expressing *Xenopus laevis* oocytes after preincubation in pH 7.1 (grey bar) with or without the indicated peptide or peptide combination (green bar); in (B) control currents (after pH 7.4 conditioning) are shown in grey for comparison. Asterisk in (C) indicates significant difference to control condition ($p = 0.0001$); $n = 5$-68). (D) Concentration-response curves for activation (Act.) and SSD of WT ASIC1a in the presence and absence of 100 nM BigDyn ($n = 4$-15). (E) Structure of cASIC1a (PDB: 4NTW) with individual subunits color coded and inset showing the location of K105. (F) Representative current (black) and fluorescence (red) traces obtained by application of pH 5.5 (black bars) at mASIC1a labeled with Alexa Fluor 488 at position 105, the indicated peptide (PcTx1: blue bar; BigDyn: dark green bar and DynB: light green bar) or pH 9.0 (purple bar). (G) Averaged change in fluorescence obtained by application of PcTx1, BigDyn, DynB or pH 9.0, as shown in (F) (normalized to that obtained by application of pH 5.5) ($n = 5$-15). Error bars in (C), (D) and (G) represent 95CI.

possibilities, we turned to voltage-clamp fluorometry, which allows us to directly probe ion channel conformational rearrangements using environmentally sensitive fluorescent dyes (21). In agreement with earlier reports (22), Alexa Fluor 488-labelled Lys105Cys mutants (Figure 1E) showed robust and reversible pH-induced current and fluorescence changes (Figure 1F, Table S2). The upward deflection of the fluorescence signal is likely associated with channel desensitization, as the pH response curve of the fluorescence closely matches that of SSD (Figure S2, Table S3). Additionally, application of 0.3 μM tarantula toxin PcTx1, reported to stabilize the desensitized state of ASIC1a by increasing the proton sensitivity (23, 24) through binding to the acidic pocket (25, 26), also induces an upward deflection in fluorescence without inducing current (Figure 1F-G). By contrast, application of 1 μM BigDyn did not result in a current response, but caused a downward deflection (quenching) of the fluorescence signal, in stark contrast to the upward deflection (dequenching) observed with increased proton concentrations and PcTx1. Importantly, no fluorescence change was observed upon application of 1 μM DynB or increasing the pH to 9.0 (Figure 1F-G, Table S2), demonstrating that the BigDyn-induced conformation is dependent on a functionally active peptide and distinct from that elicited by low (or high) pH. Together, the data show that mASIC1a modulation by BigDyn is dependent on a continuous peptide sequence containing, at least parts of, both DynA and DynB and that BigDyn likely stabilizes a closed resting conformation of ASIC1a that is distinct from that induced by protons and PcTx1.

Contribution of positively charged BigDyn side chains to modulation of ASIC1a

An unusual feature of BigDyn is its high density of positive charge (net charge +9, Figure 2A). We therefore reasoned that the interaction with ASIC1a might be driven by electrostatic forces, i.e. by binding to negatively charged side chains on ASIC1a. To investigate the contribution of individual positively charged amino acids (Arg and Lys) of BigDyn to its ability to modulate ASIC1a SSD, we generated BigDyn analogs with individual positively charged residues substituted for alanine (Ala). These ten BigDyn Ala-analogs were tested for their

ability to rescue current at WT mASIC1a when applied at 1 µM at a conditioning pH of 7.1 (Figure 2B-C). Indeed, individual alanine substitutions of the three most N-terminally located positively charged amino acids (Arg6, Arg7 and Arg9) virtually abolished BigDyn-mediated current rescue: 9.8 % (95CI: -2.1, 21.6 %) for Arg6Ala, 5.0 % (95CI: 1.2, 8.7 %) for Arg7Ala, and 2.3 % (95CI: 1.7, 3.0 %) for Arg9Ala, respectively (Table S4).

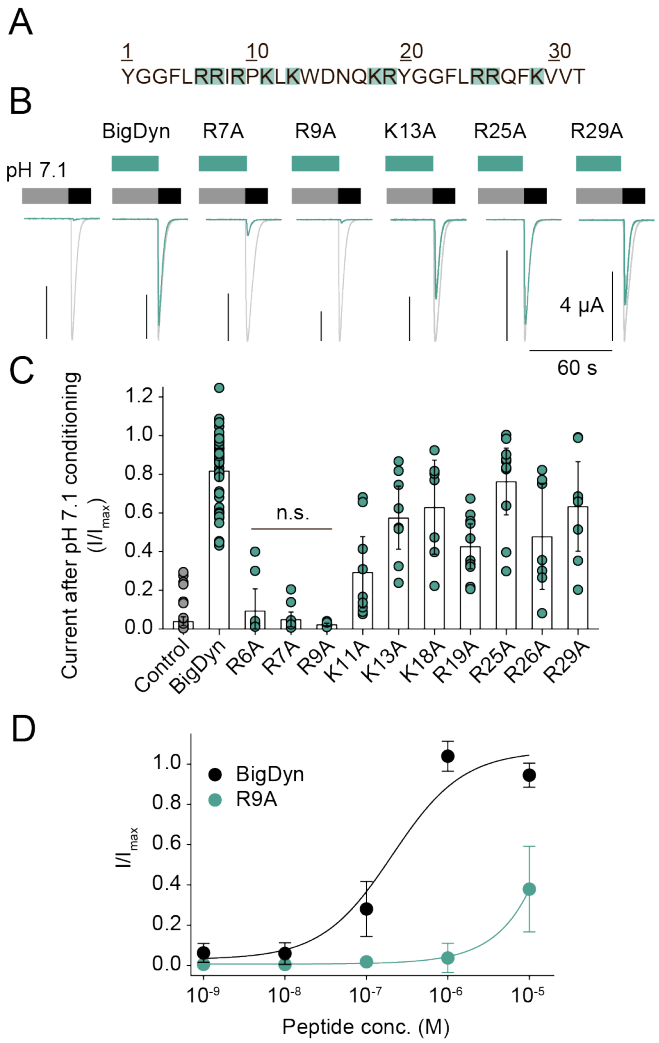

Figure 2: Positive charges near the BigDyn N-terminus are essential for ASIC1a modulation. (A) Sequence of BigDyn with basic side chains highlighted in green. (B/C) Representative current traces (B) and averaged data (C) obtained by pH 5.6 application (black bar in (B)) at ASIC1a WT-expressing *Xenopus laevis* oocytes after preincubation in pH 7.1 (grey bar) with or without the indicated BigDyn analog (green bar); control currents after pH 7.6 conditioning are shown in grey for comparison (B). (D) Concentration-response curves for WT ASIC1a modulation by BigDyn (black) and R9A (blue). Error bars in (C) and (D) represent 95CI. In (C), n.s. indicates no statistical significant difference to control condition. n = 7-48 in (C) and n = 7-9 in (D).

By contrast, individual substitution of the remaining positive charges (Lys11, Lys13, Lys18, Arg19, Arg25, Arg26, and Lys29; Figure 2) or the residue situated between Arg7 and Arg9 (Ile8; Figure S3A) showed less pronounced effects on BigDyn activity (between 29.4-76.3 % recovery; Table S4). This indicates that the charge of a cluster of three closely positioned Arg in the N-terminal part of BigDyn is important for the functional modulation of mASIC1a, although other properties, such as side chains size and H-bonding ability might also play a role (Figure 2). This notion is confirmed by the finding that the EC_{50} for the modulatory effect of the Arg9Ala peptide is increased over 50-fold (Figure 2D). Consistent with the above, substituting the sole negative charge (Asp15) had no effect on its ability to modulate ASIC1a (Figure S3A). Replacing Tyr1, which has been implicated in the activity of BigDyn towards the opioid receptor (27-29), or Trp14, resulted in a modest, but significant decrease in the ability to rescue currents (Figure S3A), while N-terminal truncations generally had more pronounced effects (Figure S3B, Table S5).

Together, the data indicate that the BigDyn-mediated effects on ASIC1a are primarily driven by a cluster of three positively charged side chains in the N-terminal part of the neuropeptide.

Negative charges within the acidic pocket are crucial for BigDyn modulation of ASIC1a

To complement our findings with BigDyn, we next wanted to identify its binding site on ASIC1a. As we found the basic charge of BigDyn to be a crucial determinant of the interaction, we set out to mutate negatively charged side chains in the mASIC1a extracellular domain (ECD). Specifically, we focused our attention on a cavity in the ASIC1a ECD denoted the acidic pocket, which contains a high density of negatively charged residues (30). The acidic pocket also serves as the binding site of PcTx1 (25, 26, 31), which has been suggested to compete with BigDyn for ASIC1a modulation (10). We introduced charge-neutralizing amino acid substitutions to individual acidic side chains (Asp to Asn and Glu to Gln substitutions) at eight positions in and around the acidic pocket (Figure 3A). As

ASIC1a mutations, especially around the acidic pocket, often lead to a change in pH sensitivity, the pH dependence of SSD for each of the mutant mASIC1a constructs was determined in order to identify the appropriate SSD conditioning pH for each mutant (Figure S4, Table S6). Next, we tested the mASIC1a variants for their sensitivity towards 1 µM BigDyn, applied during SSD conditioning. However, all tested single mutants retained significant pH 5.6-induced current rescue (Figure 3B-C, Table S7), indicating that single charge-neutralizing amino acid substitutions in or near the acidic pocket alone are not enough to abolish the effect of BigDyn.

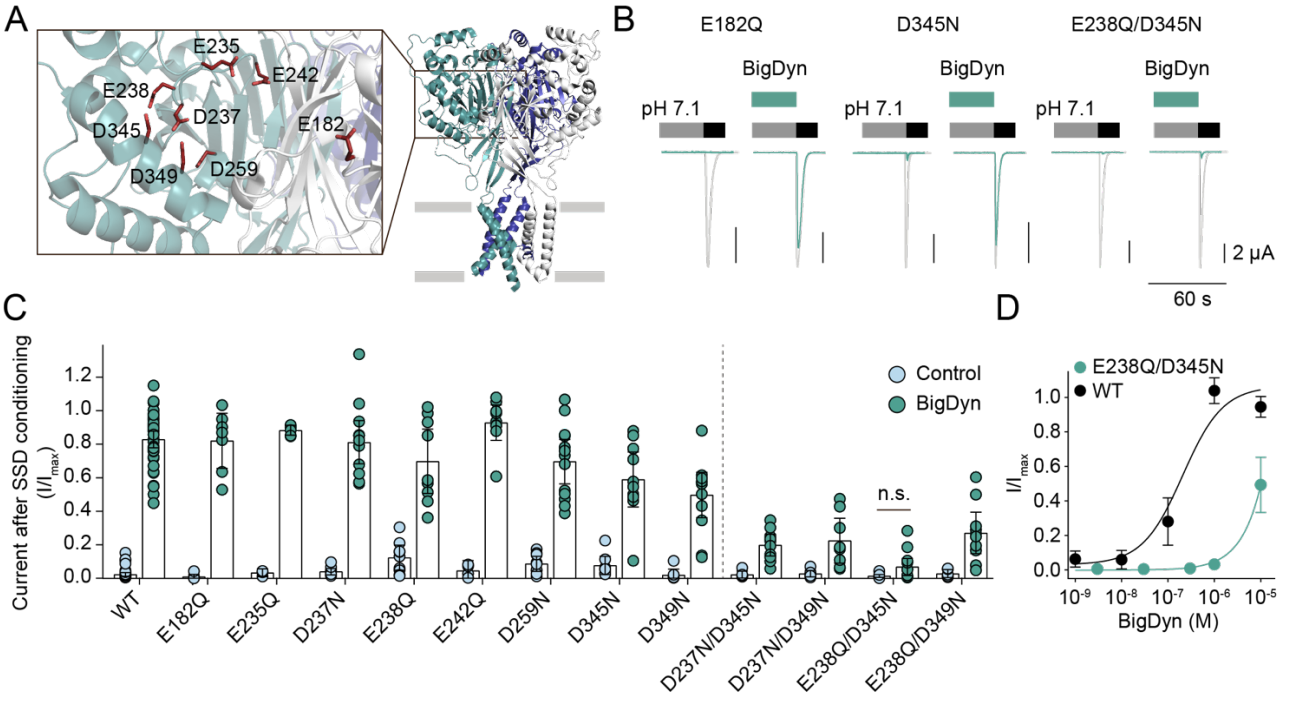

Figure 3: Double-charge neutralizing mutations around ASIC1a acidic pocket reduce BigDyn modulation. (A) Structure of cASIC1a (PDB: 4NTW) with individual subunits color coded and inset showing the location of acidic side chains mutated to Gln or Asn. (B/C) Representative current traces (B) and averaged data (C) obtained by pH 5.6 application (black bar in (B)) after preincubation in SSD-inducing pH (grey bar; see Fig S4 and Table S6 for details) with or without BigDyn (green bar) at *Xenopus laevis* oocytes expressing the indicated ASIC1a construct; in (B) control currents after pH 7.6 conditioning are shown in grey for comparison (n = 4-45). (D) Concentration-response curves for BigDyn-mediated modulation of WT (black) and E238Q/D345N mutant (green) ASIC1a (n= 7-9). Error bars in (C) and (D) represent 95CI. In (C), n.s. indicates no statistical significant difference to control condition.

We therefore sought to investigate whether combined mutation of two acidic residues in the acidic pocket would abolish BigDyn modulation. Four acidic residues are found in close proximity on the upper thumb and finger domains, (Asp237, Glu238, Asp345, and Asp349; Figure 3A) and have been suggested to interact as two carboxyl-carboxylate pairs (Asp237-Asp349 and Glu238-Asp345) (30). We thus generated mASIC1a variants carrying a combination of two charge-neutralizing Asp to Asn and/or Glu to Gln mutations of these four residues and measured their pH dependence of steady-state desensitization (Figure S4 and Table S6). The double mutant mASIC1a constructs were then tested for their sensitivity to BigDyn modulation using the same protocol as for the single mutations, except that Asp237Asn/Asp345Asn was activated at pH 4.0 in order to reach saturating currents. All four tested acidic pocket double mutants showed a drastically decreased sensitivity to 1 μM BigDyn compared to WT mASIC1a (Figure 3B-C and Table S7). The biggest decrease in rescue of pH 5.6-induced currents was observed for Glu238Gln/Asp345Asn ASIC1a. For this construct, application of 1 μM BigDyn during SSD conditioning resulted in 6.8 % (95CI: 1.7, 11.8 %) current compared to pH 5.6-induced currents after pH 7.6 conditioning, which was comparable to the control response observed in absence of BigDyn (Figure 3B-C). Additionally, the Glu238Gln/Asp345Asn double mutant showed a roughly 50-fold increase in the EC_{50} for the modulatory effect of BigDyn (Figure 3D). As the Hill slope of ASIC1a SSD is unusually steep, we sought to confirm that the loss of the BigDyn effect observed for the double mutants was not due to a shift in pH sensitivity that rendered the channels overall unresponsive. As detailed in Figure S5A and Table S7, this was not the case, although the Asp237Asn/Asp349Asn mutant showed a moderately reduced effect when a different conditioning pH was employed.

Next, we wanted to ascertain that the loss of BigDyn modulation is indeed specific to double charge-neutralizing mutations in or near the acidic pocket. We thus tested two additional double charge-neutralizing mutations at positions outside the acidic pocket, Asp253Asn/Glu245Gln and Glu373Gln/Glu411Gln (Figure S5B-C). Both double mutants

retained full sensitivity towards 1 μM BigDyn, indicating that the effect of double charge neutralizing mutants was specific to the acidic pocket.

In principle, it is possible that the observed loss of current rescue with the double charge-neutralizing mutations in or near the acidic pocket originates from a changed desensitization profiles. However, this is highly unlikely, given that there was no correlation between the extent of change in SSD and current rescue and mutants with WT-like or even left-shifted SSD curves showed a drastic loss of current recue (e.g. Glu238Gln/Asp345Asn and Glu238Gln/Asp349Asn). Overall, the data therefore strongly imply that the acidic pocket serves as an interaction site for BigDyn.

Photocrosslinking confirms an interaction site in the acidic pocket

To further validate the acidic pocket as the BigDyn binding site, we turned to UV-induced photocrosslinking using the photoreactive side chain of the non-canonical amino acid (ncAA) azido-phenylalanine (AzF) incorporated at different positions in ASIC1a (Figure 4A-B) (32-34). Incorporating AzF at positions lining the ASIC1a-BigDyn interaction interface should allow covalent trapping of the complex and enable subsequent visualization using western blotting. To this end, we removed endogenous ASIC1a from HEK 293 cells by CRISPR/Cas9 and expressed hASIC1a variants carrying AzF at Glu177, Thr236, Thr239, Lys 343, Glu344, Asp351, Glu355, Lys356 and Asp357 respectively, using the non-sense suppression methodology (Figure 4A-B) (35). Efficient ncAA incorporation was confirmed through much larger amounts of protein from cells grown in presence compared to cells grown in the absence of AzF (Figure S6A-B). Notably, while SSD of hASIC1a is shifted compared to that of mASIC1a (hASIC1a pH_{50} SSD: 7.07 (95CI: 7.03, 7.11) *vs.* mASIC1a pH_{50} SSD 7.24 (95CI: 7.23, 7.25)) (36), the modulatory effect of BigDyn on the human ortholog is virtually identical (Figure S6C-E). As shown in Figure 4C, covalently crosslinked BigDyn was detected in samples containing AzF in and around the acidic pocket only when they were exposed to UV light, but not in control samples processed in absence of UV light or in UV-

exposed WT hASIC1a, or when AzF was incorporated in the lower parts of the ECD, i.e. away from the acidic pocket (Tyr71 and Trp287). In summary, incorporation of the ncAA AzF in combination with UV-induced photocrosslinking confirmed that the BigDyn binding site is located at the ASIC1a acidic pocket.

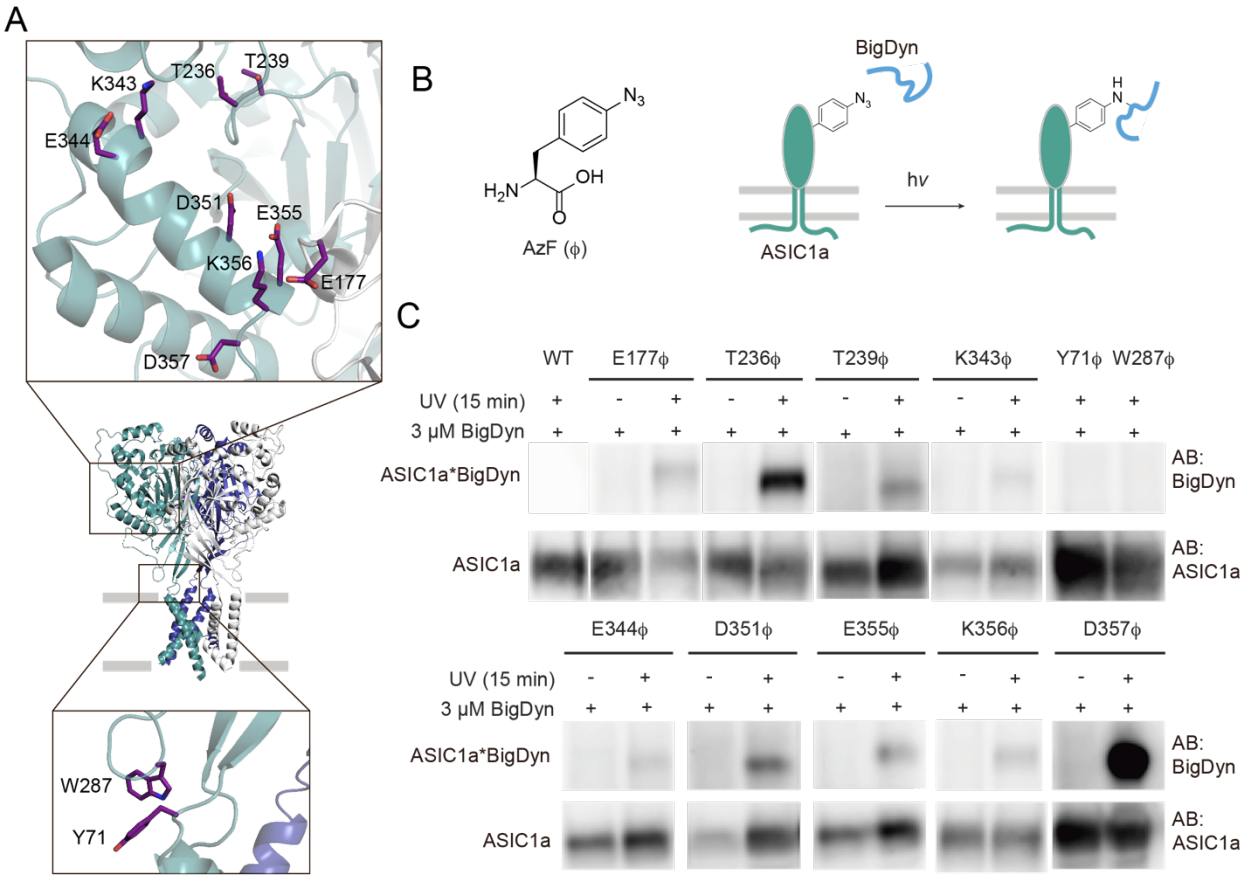

Figure 4: Photocrosslinking confirms the BigDyn interaction site at the acidic pocket. (A) Structure of cASIC1a (PDB: 4NTW) with individual subunits color coded and inset highlighting side chains replaced by 4-Azido-L-phenylalanine (ϕ) in the acidic pocket (upper inset) and lower extracellular domain (lower inset). (B) Structure of 4-Azido-L-phenylalanine (AzF, ϕ) and schematic workflow for crosslinking to BigDyn. HEK 293 cells expressing ϕ-containing ASIC1a variants are incubated with 3 μM BigDyn and exposed to UV light for 15 min to form covalent ASIC1a-BigDyn complexes. The complex is purified via a C-terminal 1D4 tag on ASIC1a and visualized via western blotting. (C) Western blot of purified hASIC1a WT and variants carrying ϕ in the extracellular domain. BigDyn is detected only in UV-exposed samples containing ϕ in the acidic pocket, but absent in control samples not exposed to UV, those carrying ϕ in the lower extracellular domain (lower inset in (A)) or WT. See also Figure S7.

Discussion

Mechanism of action of BigDyn on ASIC1a

Despite the potential pathophysiological relevance of the ASIC-BigDyn interaction (10), the determinants for the high-potency modulation of ASIC SSD by BigDyn have remained enigmatic. A defining characteristic of neuropeptide signaling is its slow time scale relative to the fast transmission achieved by small-molecules (1, 2). Indeed, we and others have found that the functional effects of BigDyn on ASIC1a-mediated currents require relatively long preincubation times ((10) and Figure 1). The notion of a slow binding and unbinding process is directly supported by our voltage-clamp fluorometry data, which demonstrate that BigDyn-induced conformational changes are drastically slower than those induced by changes in proton concentration (Figure 1). Once bound, BigDyn reduces the proton sensitivity of both pH-dependent activation and SSD of ASIC1a. Although the acidic pocket is not likely to be the primary proton sensor of ASICs (37, 38), side chains in and around the acidic pocket have been shown to modulate proton sensitivity (30, 37). A direct binding of BigDyn to this region is therefore expected to alter proton sensing. Interestingly, our data suggest that BigDyn binding favors a resting closed state that is distinct from open and desensitized states induced by protons (or PcTx1). In other words, the BigDyn-induced conformation increases the energetic barrier to populate both open and desensitized states, consistent with the right-shift of both parameters in the presence of BigDyn (Figure 1). In the case of SSD, this would result in ASIC1a remaining responsive to pH drops even during proton concentrations that would normally desensitize the channel, thus explaining the ability of BigDyn to noticeably increase ASIC1a dependent neuronal death during acidosis (10).

As activation and desensitization both involve the collapse of the acidic pocket, bringing thumb and finger domain aspartate side chains from ~8 Å to within <3 Å of each other (39), we speculate that BigDyn binding hinders the proton-induced transitions from resting closed states to active and/or desensitized states.

Defining site of the ASIC1a-BigDyn interaction

Consistent with the hypothesis that the unusually high density of positive charge of BigDyn is crucial for its functional effects, we find that charge-neutralizing mutations of basic amino acids reduce the ability of BigDyn to rescue ASIC1a proton-gated currents after exposure to steady-state desensitization (SSD)-inducing conditions. This effect was particularly pronounced for mutations in a cluster of three Arg (Arg6, Arg7 and Arg9) in the N-terminal part of the peptide, while no effect was observed when mutating the only non-charged side chain in between amino acids 6 and 9 (Ile8). This is in agreement with the finding that DynA (representing the N-terminal part of BigDyn), but not DynB (representing the C-terminal part of BigDyn) can have modulatory effects on ASICs (10, 40) (Figure S1C). However, it is worth noting that functional effects were also reduced when mutating Lys11, Arg19, Arg26 and Tyr1, albeit to a lesser extent (Figure 2 and S3A). These data suggest that the interaction of BigDyn with ASIC1a is not solely driven by charge at Arg6, Arg7 and Arg9, but also mediated by other, mostly basic amino acids throughout the peptide sequence. This notion is further supported by data from our N-terminal truncation screen and complemented by the finding that AzF incorporated at positions along the entire length of the cleft formed by the acidic pocket enabled to covalently crosslink to BigDyn. Together, this argues for an extended interaction surface on ASIC1a, likely extending from the peripheral thumb domain around the α5 helix and into the acidic pocket. While the location of the BigDyn binding site is distinct from that suggested for RFamide neuropeptides on ASICs (41, 42), it does overlap with the binding site for PcTx1 (10, 25, 26, 31). This is consistent with the finding that RFamides do not functionally compete with BigDyn or PcTx1 (10, 43). Interestingly, both PcTx1 and BigDyn bind to the acidic pocket through extensive charge-charge interactions, and additional contributions are made by aromatic amino acids (i.e. Trp7 and Trp24 in PcTx1 (31) and Tyr1 in BigDyn). However, the binding mode is likely to differ substantially between the two peptides, as PcTx1 adopts a rigid fold, while BigDyn is likely unstructured in aqueous

solution (44, 45). Indeed, the two peptides have opposite modulatory effects on ASIC1a: while PcTx1 interacts with and stabilizes the desensitized state (24), our data suggest that BigDyn stabilizes a closed/resting state of ASIC1a (see above).

Possible biological implications

Intriguingly, both ASIC1a and dynorphins have been shown to exhibit overlapping expression patterns (e.g. amygdala, hippocampus) and to contribute to a similar array of both physiological (learning, memory) and pathophysiological (pain, nociception, addiction) processes (4, 5, 11, 12, 46-52). Among the dynorphins tested here, BigDyn is the most potent at ASIC1a and has also been shown to greatly enhance acidosis-induced cell death in cortical neurons (10). The potential relevance of this finding is underscored by the fact that under pathophysiological conditions, the BigDyn levels will be sufficient to modulate ASIC activity *in vivo* (up to low micromolar range) (4, 5, 8, 10, 53, 54). By contrast, the modulatory effects under physiological BigDyn concentrations (1-10 nM) would likely be small, although others have reported a higher sensitivity of ASIC1a towards BigDyn (10). Together, this highlights the potential of the ASIC-BigDyn interaction site as a drug target. Given that BigDyn and PcTx1 share a common binding site, this notion is supported by the finding that PcTx1 or PcTx1-like peptides show promise in limiting neuronal death in stroke models (14, 15). While the ASIC-BigDyn interaction *per se* increases neuronal death, a therapeutic option might in the future emerge from building upon the scaffold of modified peptides with reduced activity (similar to some presented in this study) that could, if refined, work as silent modulators to prevent the ASIC–BigDyn interaction. Recent work on PcTx1 has shown that peptides targeting the ASIC acidic pocket can display significant functional plasticity. For example, altered pH or mutations within the toxin (Arg27Ala or Phe30Ala) can effectively convert PcTx1 into a potentiator) (31, 55). Similarly, and depending on cellular context and presence of co-factors, DynA can act as both an inhibitor and potentiator of glutamate

receptors (4). It will thus be intriguing to see if this functional dichotomy is also possible to achieve for BigDyn in order to unlock its potential as an ASIC-targeting therapeutic lead.

Methods

Molecular biology

The complementary DNA (cDNA) encoding mouse ASIC1a (mASIC1a) was used as previously described (56), while the human ASIC1a (hASIC1a) cDNA was kindly provided by Dr Stephan Kellenberger. Plasmids containing AzF RS and tRNA were gifts from Dr Thomas P. Sakmar (32). The dominant negative eukaryotic release factor (DN-eRF) was a gift from Dr William Zagotta (57).

Site-directed mutagenesis was performed using PfuUltraII Fusion polymerase (Agilent) and custom DNA mutagenesis primers (Eurofins Genomics). All sequences were confirmed by sequencing of the full coding frame (Eurofins Genomics). For hASIC1a constructs, a C-terminal 1D4-tag was added for protein purification and Western blot detection and two silent mutations were inserted at V10 and L30 to reduce the risk of potential reinitiation (58). cDNAs were linearized with EcoRI (mASIC1a) or HindIII-HF (hASIC1a, both New England Biolabs) and capped cRNA was transcribed with the Ambion mMESSAGE mMACHINE SP6 (mASIC1a) kit (Thermo Fisher Scientific).

Electrophysiological recordings and data analysis

Oocytes were surgically removed from adult female *Xenopus laevis* and prepared as previously described (56). Oocytes were injected with 0.1 to 10 ng cRNA of mouse ASIC1a (mASIC1a) or hASIC1a mRNA into the cytosol (volumes between 9 and 50 nL). Typically, higher amounts of mutant mASIC1a constructs were injected compared WT mASIC1a. 1-4 days after injection, oocytes were transferred to a recording chamber (59), continuously perfused (2.5 mL/min) with bath solution containing (in mM): 96 NaCl, 2 KCl, 1.8 $BaCl_2$, 2 $MgCl_2$, and 5 HEPES, pH adjusted by NaOH or HCl. Solutions exchange was achieved using a gravity-driven 8-line automated perfusion system operated by a ValveBank module (AutoMate Scientific). Current recordings were performed in presence of 0.05% bovine serum albumin (≥ 98% essentially fatty acid-free, Sigma Aldrich). Currents were recorded

using microelectrodes (borosilicate capillaries 1.2 mm OD, 0.94 mm ID, Harvard Apparatus), backfilled with 3 M KCl (0.5-2 MΩ) and an OC-725C amplifier (Warner Instruments). The current signal was acquired at 500 Hz, filtered by a 50-60 Hz noise eliminator (Hum Bug, Quest Scientific) and digitized using an Axon™ Digidata® 1550 Data Acquisition System and the pClamp (10.5.1.0) software (Molecular Devices). The current signal was further digitally filtered at 2.8 Hz using an 8-pole Bessel low-pass filter prior to analysis. Displayed current traces have been subjected to additional 50× data reduction.

Synthetic PcTx1 was obtained from Alomone Labs (>95 % purity). PcTx1 and synthetized dynorphin peptides and analogs stock solutions were prepared in MilliQ (18.2 MΩ resistivity). Peptide stock solutions were stored at -20 °C. Prior to recording, the peptides were diluted to the desired concentration in recording solutions.

Concentration-response relationships of wt mASIC1a activation were determined by 20 s applications of solutions with decreasing pH-values. Between each 20 s application, the oocytes were left to recover for 2 min in pH 7.4 solution (unless stated otherwise). The currents elicited by the 20 s application of acidic pH were normalized to the largest current size for each of individual oocyte tested. Steady-state desensitization (SSD) concentration-response relationships were determined by exposing ASIC1a expressing oocytes to a 20 s application of pH 5.6 (unless stated otherwise), while decreasing the resting pH in between applications of pH 5.6. The resting period between pH 5.6 applications was 2 min. In order to ensure that the observed current desensitization was not due to general current run-down, a final application of pH 5.6 was performed after a 2 min resting period at a resting pH that resulting in saturating current responses. Traces were used for further analysis only if the final pH 5.6 application resulted in currents that were ≥ 80 % of the same resting pH prior to the SSD protocol.

The ability of dynorphin peptides to rescue ASIC1a proton-gated currents after exposure to SSD-inducing conditions was examined at a resting pH of 7.6 (unless stated otherwise). Channel activation was achieved by application of pH 5.6 (except for D237N/D345N and

E373Q/E411Q construct which required pH 4.0 for full activation) for 20 s. The oocytes were left to recover for 1 min in pH 7.6 solution. Hereafter, the oocyte was perfused for 2 min with SSD-inducing pH (determined specifically for each individual ASIC1a construct/mutant) prior to a 20 s application of pH 5.6. Dynorphin peptides were applied during the 2 min of SSD conditioning. The channels were checked for ability to recover (cutoff at ≥80 % recovery) after 3 min of pH 7.6 solution by an additional 20 s application pH 5.6. The effect of the dynorphin peptides was determined by normalizing the current post-peptide application to the mean of the two currents elicited without SSD conditioning pH.

Voltage-clamp fluorometry

For voltage-clamp fluorometry (VCF), 5-20 ng of mASIC1a K105C mRNA were injected into oocytes which were then incubated for 2-7 days. On the day of the recording, oocytes were labeled by incubating them for 30 min with 10 μM AlexaFlour 488 C5-maleimide (Thermo Fisher Scientific) in OR2 solution at room temperature, subsequently washed twice with OR2, and stored in the dark until further use. The oocytes were placed in the custom-built recording chamber above a water immersion objective of an inverse microscope (IX73 with LUMPlanFL N 40x, Olympus), with the animal pole facing the excitation source. An Olympus TH4-200 halogen lamp using a standard GFP filter-set (Olympus) was used to excite the fluorophore while the emission was detected using a P25PC-19 photomultiplier tube (Sens-Tech) and photon-to-voltage converter (IonOptix), via the microscope side port. Current and fluorescence signals were acquired, filtered, digitized and digitally filtered as described for the other electrophysiology recordings.

For VCF measurements in Fig 1F-G, 0.05% BSA was added to all solutions (composition as described above). Channels were activated for 20 s using pH 5.5 buffer, washed for 1 min with pH 7.6 buffer, exposed for 2 min to 0.3 μM PcTx, 1 μM BigDyn or DynB at pH 7.6 respectively, followed by a 2 min washout at pH 7.6 and a subsequent 20 s exposure to pH 5.5. For the pH response curve in SI Figure S2, oocytes were exposed for 20 s to pH 6.0,

washed for 1 min at pH 7.6, exposed for 1-2 min (until fluorescent signal reached a plateau) with preconditioning pH 7.2, followed directly by exposure to pH 6.0. After a 1min washout at 7.6 this protocol was consecutively repeated using decreasing preconditioning pHs (7.1, 7.0, 6.8, 6.6), in the end the response to pH 6.4 was measured. All signals were reported relative to deflections at pH 6.0 for the pH-response curve in SI Figure S2 and relative to deflections at pH 5.5 for experiments in Figure 1F-G. Fluorescent signal intensity was reported as percentage change relative to the baseline fluorescence level and the fluorescent baseline was adjusted for traces in Figure 1F.

Cell culture and transfection

HEK 293T cells (ATCC®) were grown in monolayer in T75 and T175 flasks (Orange Scientific) in DMEM (Gibco) supplemented with 10 % FBS (Thermo Fisher Scientific) and 1 % penicillin-streptomycin (Thermo Fisher Scientific) and incubated at 37 ˚C in a humidified 5 % CO_2 atmosphere. Endogenous hASIC1a was removed by CRISPR/Cas9 using the guide RNA published in (60). For crosslinking studies, cells were seeded into 15 cm dishes (VWR) at a density of 5-7 mio. cells and transfected the next day with PEI (Polysciences) and 16:4:4:8 µg DNA encoding hASIC1a TAG variants, AzFRS, tRNA and DN-eRF, respectively. For the WT control, 2 mio cells were seeded into a 10 cm dish (VWR) and transfected with 8 µg hASIC1a WT. Six hours after transfection, cell medium was replaced with DMEM containing 0.5 mM AzF (4-Azido-L-phenylalanine, Chem Impex) and crosslinking studies were performed 48 hours after transfection.

Crosslinking studies, protein purification, Western blotting

Cells were washed with PBS and dislodged from the dishes using cell scrapers (Orange Scientific). After centrifugation at 1000 rpm for 5 min, cell pellets were resuspended in 1 ml PBS containing 3 µM BigDyn (pH 7.4) and transferred into 12 well plates (Orange Scientific). Cells were crosslinked under a Maxima ML-3500 S UV-A light source (Spectronics

corporation, 365 nm) for 15 min on ice. Control samples without UV exposure were kept at 4 °C. After crosslinking, cells were centrifuged at 1000 rpm for 5 min and resuspended in 1 ml solubilisation buffer (50 mM Tris-HCl, 145 mM NaCl, 5 mM EDTA, 2 mM DDM, pH 7.5) supplemented with cOmplete™ EDTA-free protease inhibitor cocktail (Sigma Aldrich). Cells were lysed at 4 °C for 2 h and centrifuged at 18000 g and 4 °C for 30 min. In parallel, 40 µl Dynabeads Protein G (Thermo Fisher Scientific) were washed with 200 µl PBS/0.2 mM DDM and incubated with 4 µg RHO 1D4 antibody (University of British Columbia) in 50 µl PBS/0.2 mM DDM for 30 min on a ferris wheel (VWR). After washing the beads with 200 µl PBS/0.2 mM DDM, the cell lysate supernatant was incubated with the beads on the ferris wheel at 4 °C for 90 min. Beads were washed with 200 µl PBS three times to remove nonspecifically bound proteins and incubated in 25 µl elution buffer (2:1 mixture between 50 mM glycine, pH 2.8 and 62.5 mM Tris-HCl, 2.5 % SDS, 10 % Glycerol, pH 6.8) supplemented with 80 mM DTT at 70 °C for 10 min. Protein samples (12 µl) were mixed with 3 µl 5 M DTT and 5 µl 4x NuPAGE™ LDS sample buffer (Thermo Fisher Scientific) and incubated at 95 °C for 20 min before SDS-PAGE using 3–8 % Tris-Acetate protein gels (Thermo Fisher Scientific). After transfer onto PVDF membranes (iBlot 2 Dry Blotting System, Thermo Fisher Scientific) and blocking in TBST/3% non-fat dry milk for 1 hour, hASIC1a was detected using RHO 1D4 antibody (1 µg/µl, University of British Columbia) and 1:5000 goat anti-mouse IgG HRP-conjugate (Thermo Fisher Scientific). BigDyn was detected using 1:1000 rabbit anti-DynA antibody (abcam) and 1:5000 goat anti-rabbit IgG HRP-conjugate (Promega).

Solid-phase peptide synthesis

Unless otherwise stated, all amino acids and reagents were purchased from either Iris Biotech, Gyros Protein Technologies or Sigma Aldrich. All solvents were purchased from commercial sources and used without further purification. The molecular mass of the peptides spectra was obtained by electron spray ionization (ESI) liquid chromatography mass spectrometry (LC-MS) coupled to an Agilent 6410 Triple Quadrupole Mass with a

reverse phase C18 column (Zorbax Eclipse XBDC18, 4.6 × 50 mm) using a binary buffer system consisting of H_2O:CH_3CN:formic acid (A, ratio 95:5:0.1; B, ratio 5:95:0.1) at 0.75 mL/min. Peptide purity was determined by UV absorbance at 214 nm on an analytical reverse phase ultraperformance liquid chromatography (RP-UPLC) (Waters) system with a C18 column (Acquity UPLC BEH C18, 1.7 µm 2.1 × 50 mm) using a binary buffer system consisting of H_2O:CH_3CN:trifluoroacetic acid (TFA) (A, ratio 95:5:0.1; B, ratio 5:95:0.1) at 0.45 mL/min.

Peptides were synthesized by Fmoc solid-phase peptide synthesis (SPPS) at 0.04-0.10 mmol scale. For SPPS, preloaded 4-benzyloxybenzyl alcohol (Wang) (Iris Biotech), TentaGel® R PHB or preloaded Fmoc-Thr(OtBu) TentaGel® R PHB (Rapp Polymere) resins (100-200 mesh) were used. Loading of hydroxy-functionalized TentaGel® R PHB resin was carried out by the MSNT/MeIm (1-(2-mesitylenesulfonyl)-3-nitro-1H-1,2,4-triazole/1-methylimidazole) method (61). Loading of resin was checked spectrophotometrically, quantifying the amount of Fmoc released upon cleavage as previously described (62). Standard coupling reactions were carried out at room temperature (RT) under agitation using a mixture of Fmoc-protected amino acid derivative (4.0 equiv. relative to resin loading), N,N,N′,N′-tetramethyl-O-(1H-benzotriazol-1-yl)uranium hexafluorophosphate (HBTU, 4.0 equiv.) and N,N-diisopropylethylamine (DIPEA) (8.0 equiv.) in dimethylformamide (DMF). Coupling reactions were monitored using a Kaiser test kit (Sigma Aldrich). Fmoc deprotections were carried out by treatment with 20 % piperidine in DMF (2 × 2 min). After coupling or Fmoc deprotection steps, the resin was extensively washed with DMF.

Automated peptide synthesis was carried out using either a Prelude® X peptide synthesizer equipped with induction heating (Gyros Protein Technologies) or using a Syro Wave™ Parallel Peptide Synthesizer (Biotage). For Prelude X synthesis all reagents were prepared in DMF: Fmoc-protected amino acid (0.2 M), O-(1H-6-chlorobenzotriazole-1-yl)-1,1,3,3-tetramethyluronium hexafluorophosphate (HCTU) (0.5 M) DIPEA (1 M) and Fmoc deprotection solution (20% piperidine, v/v). Sequence elongation was achieved by following

protocol: Fmoc deprotection (2 × 2 min, 20 % piperidine (v/v), rt,) and coupling (2 × 5 min, 75 °C, for Cys couplings 2 × 5 min, 50 °C, and for Arg couplings 3 × 5 min, 50 °C). Amino acids were double coupled using amino acid:HCTU:DIPEA (ratio 1:1.25:2.5) in 5-fold excess over the resin loading to ensure efficient peptide elongation. Final Fmoc deprotection after peptide elongation (2 × 5 min) was followed by dichloromethane (DCM) wash.

For Syro Wave™ synthesis Fmoc-amino acids (0.5 M), HBTU (0.48 M) and piperidine (40 % v/v) were prepared in DMF. DIPEA (2 M) was prepared in N-methyl-2-pyrrolidone (NMP). Sequence elongation was achieved using following protocol: Fmoc deprotection (1 × 3 min treatment with 40 % piperidine in DMF followed by 1 × 12 min treatment in 20 % piperidine) and coupling (1 x 40 min, RT, for Arg and Cys couplings 2 x 40 min, RT). Amino acids were coupled using amino acid:HBTU:DIPEA (ratio 1:1:2) in 5-fold excess over the resin loading. After deprotection, the resin was washed with DMF (× 2), DCM (× 1), and DMF (× 2) for 1 min each. The final Fmoc-deprotection was achieved by treatment with 40 % piperidine in DMF (3 min), followed by treatments with 20 % piperidine in DMF (2 × 8 min).

Global deprotection and cleavage was conducted in a mixture of TFA:triisopropylsilane (TIPS):H_2O (ratio 95:2.5:2.5, v:v:v) for 2 h at room temperature. Subsequently, the cleaving mixture was concentrated and the crude peptide was precipitated with ice-cold diethyl ether. The precipitate was centrifuged at 3500 x g, 5 min at 4 °C, washed with ice-cold diethyl ether and centrifuged at 3500 x g, 5 min at 4 °C, after which it was solubilized in H_2O:CH_3CN:TFA (ratio 50:50:0.1, v:v:v) and lyophilized.

Peptides were purified using either a preparative reversed-phase high-performance liquid chromatography (RP-HPLC) system (Waters) with a RP C18 column (Zorbax, 300 SB-C18, 7 µm, 21.2 × 250 mm) or an Agilent 1260 LC system equipped with a diode array ultraviolet detector and an evaporative light-scattering detector (ELSD) using a RP-C8 column (Phenomenex Luna, 5 µm, 100 Å, 21.2 × 250 mm). A linear gradient with a binary buffer system of eluent A (H_2O:CH_3CN:TFA, ratio 95:5:0.1, v:v:v) and eluent B (CH_3CN:TFA, 99.9:0.1, v:v) was applied, with a flow rate of 20 mL/min. Collected fractions were characterized by

LC-MS. Pure fractions were pooled together and lyophilized, which yielded a white, fluffy material. The purity of final peptides was determined by RP UPLC monitoring the absorbance at 214 nm and the results are listed in Table S8.

Data analysis

Data analyses were performed in Prism (8.0) (GraphPad Software). For proton concentration-response data, peak current amplitudes were plotted against pH and fitted with the Hill equation for each recording. These were averaged to give the reported means ± 95CI in the main text. For display in figures, a single fit to the average normalized responses (± 95CI) is shown. All bar diagrams and summarized data points are presented as mean ± 95CI unless stated otherwise and number of replicates (n) represent individual experimental oocytes. Results were obtained from at least two batches of oocytes unless indicated differently. An unpaired t-test was used to compare two groups. Multiple comparisons were made with one-way analysis of variance with Dunnett's comparison to a control value (e.g. comparing with WT) or with Tukey's test for multiple comparisons. A significance level of $p < 0.05$ was applied for all analyses. All graphs and illustrations were made in Prism (8.0) (GraphPad Software) and Illustrator CC (Adobe).

Acknowledgements

We acknowledge the Lundbeck Foundation (R139-2012-12390 to SAP and R218-2016-1490 to NB), the Boehringer Ingelheim Fond (to NB), the European Union's Horizon 2020 research and innovation program under the Marie Sklodowska-Curie grant agreement No 834274 (to SAH) and the University of Copenhagen for financial support.

Author contributions

CBB, NB, SAH, EPB, LMHK, TL, KS, JA and SAP designed the research; CBB, NB, SAH, YB, DW, IG, CL, TW and LMHK performed the research and analyzed the data; JA and SAP supervised the project; CBB, NB and SAP wrote the manuscript with input from all authors.

Competing interests

The authors declare to have no competing interests.

References

1. M. P. Nusbaum, D. M. Blitz, E. Marder, Functional consequences of neuropeptide and small-molecule co-transmission. Nature reviews. Neuroscience 18, 389-403 (2017).
2. A. N. van den Pol, Neuropeptide transmission in brain circuits. Neuron 76, 98-115 (2012).
3. C. Chavkin, I. F. James, A. Goldstein, Dynorphin is a specific endogenous ligand of the kappa opioid receptor. Science 215, 413-415 (1982).
4. K. F. Hauser et al., Pathobiology of dynorphins in trauma and disease. Front Biosci 10, 216-235 (2005).
5. C. Schwarzer, 30 years of dynorphins--new insights on their functions in neuropsychiatric diseases. Pharmacol Ther 123, 353-370 (2009).
6. D. Massardier, P. F. Hunt, A direct non-opiate interaction of dynorphin-(1-13) with the N-methyl-D-aspartate (NMDA) receptor. Eur J Pharmacol 170, 125-126 (1989).
7. L. Chen, Y. Gu, L. Y. Huang, The mechanism of action for the block of NMDA receptor channels by the opioid peptide dynorphin. The Journal of neuroscience : the official journal of the Society for Neuroscience 15, 4602-4611 (1995).
8. L. Chen, Y. Gu, L. Y. Huang, The opioid peptide dynorphin directly blocks NMDA receptor channels in the rat. The Journal of physiology 482 (Pt 3), 575-581 (1995).
9. S. L. Lai, Y. Gu, L. Y. Huang, Dynorphin uses a non-opioid mechanism to potentiate N-methyl-D-aspartate currents in single rat periaqueductal gray neurons. Neurosci Lett 247, 115-118 (1998).
10. T. W. Sherwood, C. C. Askwith, Dynorphin opioid peptides enhance acid-sensing ion channel 1a activity and acidosis-induced neuronal death. The Journal of neuroscience : the official journal of the Society for Neuroscience 29, 14371-14380 (2009).
11. S. Diochot et al., Black mamba venom peptides target acid-sensing ion channels to abolish pain. Nature 490, 552-555 (2012).
12. C. J. Bohlen et al., A heteromeric Texas coral snake toxin targets acid-sensing ion channels to produce pain. Nature 479, 410-414 (2011).
13. M. Mazzuca et al., A tarantula peptide against pain via ASIC1a channels and opioid mechanisms. Nature neuroscience 10, 943-945 (2007).
14. Z. G. Xiong et al., Neuroprotection in ischemia: blocking calcium-permeable acid-sensing ion channels. Cell 118, 687-698 (2004).
15. I. R. Chassagnon et al., Potent neuroprotection after stroke afforded by a double-knot spider-venom peptide that inhibits acid-sensing ion channel 1a. Proceedings of the National Academy of Sciences of the United States of America 114, 3750-3755 (2017).

16. M. Qiang et al., Selection of an ASIC1a-blocking combinatorial antibody that protects cells from ischemic death. Proceedings of the National Academy of Sciences of the United States of America 115, E7469-E7477 (2018).
17. Y. Z. Wang et al., Tissue acidosis induces neuronal necroptosis via ASIC1a channel independent of its ionic conduction. eLife 4 (2015).
18. T. W. Sherwood, K. G. Lee, M. G. Gormley, C. C. Askwith, Heteromeric acid-sensing ion channels (ASICs) composed of ASIC2b and ASIC1a display novel channel properties and contribute to acidosis-induced neuronal death. The Journal of neuroscience : the official journal of the Society for Neuroscience 31, 9723-9734 (2011).
19. I. Coin et al., Genetically encoded chemical probes in cells reveal the binding path of urocortin-I to CRF class B GPCR. Cell 155, 1258-1269 (2013).
20. J. W. Chin et al., Addition of p-azido-L-phenylalanine to the genetic code of Escherichia coli. Journal of the American Chemical Society 124, 9026-9027 (2002).
21. J. Cowgill, B. Chanda, The contribution of voltage clamp fluorometry to the understanding of channel and transporter mechanisms. The Journal of general physiology 10.1085/jgp.201912372 (2019).
22. G. Bonifacio, C. I. Lelli, S. Kellenberger, Protonation controls ASIC1a activity via coordinated movements in multiple domains. The Journal of general physiology 143, 105-118 (2014).
23. X. Chen, H. Kalbacher, S. Grunder, The tarantula toxin psalmotoxin 1 inhibits acid-sensing ion channel (ASIC) 1a by increasing its apparent H+ affinity. The Journal of general physiology 126, 71-79 (2005).
24. X. Chen, H. Kalbacher, S. Grunder, Interaction of acid-sensing ion channel (ASIC) 1 with the tarantula toxin psalmotoxin 1 is state dependent. The Journal of general physiology 127, 267-276 (2006).
25. R. J. Dawson et al., Structure of the acid-sensing ion channel 1 in complex with the gating modifier Psalmotoxin 1. Nature communications 3, 936 (2012).
26. I. Baconguis, E. Gouaux, Structural plasticity and dynamic selectivity of acid-sensing ion channel-spider toxin complexes. Nature 489, 400-405 (2012).
27. J. M. Walker, H. C. Moises, D. H. Coy, G. Baldrighi, H. Akil, Nonopiate effects of dynorphin and des-Tyr-dynorphin. Science 218, 1136-1138 (1982).
28. M. Wollemann, S. Benyhe, Non-opioid actions of opioid peptides. Life Sci 75, 257-270 (2004).
29. S. Podvin, T. Yaksh, V. Hook, The Emerging Role of Spinal Dynorphin in Chronic Pain: A Therapeutic Perspective. Annual review of pharmacology and toxicology 56, 511-533 (2016).
30. J. Jasti, H. Furukawa, E. B. Gonzales, E. Gouaux, Structure of acid-sensing ion channel 1 at 1.9 A resolution and low pH. Nature 449, 316-323 (2007).

31. N. J. Saez et al., Molecular dynamics and functional studies define a hot spot of crystal contacts essential for PcTx1 inhibition of acid-sensing ion channel 1a. British journal of pharmacology 172, 4985-4995 (2015).
32. S. Ye, T. Huber, R. Vogel, T. P. Sakmar, FTIR analysis of GPCR activation using azido probes. Nature chemical biology 5, 397-399 (2009).
33. M. H. Poulsen, A. Poshtiban, V. Klippenstein, V. Ghisi, A. J. R. Plested, Gating modules of the AMPA receptor pore domain revealed by unnatural amino acid mutagenesis. Proceedings of the National Academy of Sciences of the United States of America 116, 13358-13367 (2019).
34. H. Rannversson et al., Genetically encoded photocrosslinkers locate the high-affinity binding site of antidepressant drugs in the human serotonin transporter. Nature communications 7, 11261 (2016).
35. J. W. Chin, Expanding and reprogramming the genetic code. Nature 550, 53-60 (2017).
36. T. W. Sherwood, C. C. Askwith, Endogenous arginine-phenylalanine-amide-related peptides alter steady-state desensitization of ASIC1a. The Journal of biological chemistry 283, 1818-1830 (2008).
37. T. Lynagh, Y. Mikhaleva, J. M. Colding, J. C. Glover, S. A. Pless, Acid-sensing ion channels emerged over 600 Mya and are conserved throughout the deuterostomes. Proceedings of the National Academy of Sciences of the United States of America 115, 8430-8435 (2018).
38. S. Vullo et al., Conformational dynamics and role of the acidic pocket in ASIC pH-dependent gating. Proceedings of the National Academy of Sciences of the United States of America 114, 3768-3773 (2017).
39. N. Yoder, C. Yoshioka, E. Gouaux, Gating mechanisms of acid-sensing ion channels. Nature 555, 397-401 (2018).
40. A. Vyvers, A. Schmidt, D. Wiemuth, S. Grunder, Screening of 109 neuropeptides on ASICs reveals no direct agonists and dynorphin A, YFMRFamide and endomorphin-1 as modulators. Scientific reports 8, 18000 (2018).
41. M. Reiners et al., The Conorfamide RPRFa Stabilizes the Open Conformation of Acid-Sensing Ion Channel 3 via the Nonproton Ligand-Sensing Domain. Molecular pharmacology 94, 1114-1124 (2018).
42. B. Bargeton et al., Mutations in the palm domain disrupt modulation of acid-sensing ion channel 1a currents by neuropeptides. Scientific reports 9, 2599 (2019).
43. M. Salinas et al., The receptor site of the spider toxin PcTx1 on the proton-gated cation channel ASIC1a. The Journal of physiology 570, 339-354 (2006).
44. G. Ferre, G. Czaplicki, P. Demange, A. Milon, Structure and dynamics of dynorphin peptide and its receptor. Vitam Horm 111, 17-47 (2019).

45. C. O'Connor et al., NMR structure and dynamics of the agonist dynorphin peptide bound to the human kappa opioid receptor. Proceedings of the National Academy of Sciences of the United States of America 112, 11852-11857 (2015).
46. J. A. Wemmie, R. J. Taugher, C. J. Kreple, Acid-sensing ion channels in pain and disease. Nature reviews. Neuroscience 14, 461-471 (2013).
47. C. J. Kreple et al., Acid-sensing ion channels contribute to synaptic transmission and inhibit cocaine-evoked plasticity. Nature neuroscience 17, 1083-1091 (2014).
48. W. Wittmann et al., Prodynorphin-derived peptides are critical modulators of anxiety and regulate neurochemistry and corticosterone. Neuropsychopharmacology 34, 775-785 (2009).
49. A. Kuzmin, N. Madjid, L. Terenius, S. O. Ogren, G. Bakalkin, Big dynorphin, a prodynorphin-derived peptide produces NMDA receptor-mediated effects on memory, anxiolytic-like and locomotor behavior in mice. Neuropsychopharmacology 31, 1928-1937 (2006).
50. J. A. Wemmie et al., Overexpression of acid-sensing ion channel 1a in transgenic mice increases acquired fear-related behavior. Proceedings of the National Academy of Sciences of the United States of America 101, 3621-3626 (2004).
51. Q. Wang et al., Fear extinction requires ASIC1a-dependent regulation of hippocampal-prefrontal correlates. Sci Adv 4, eaau3075 (2018).
52. V. I. Pidoplichko et al., ASIC1a activation enhances inhibition in the basolateral amygdala and reduces anxiety. The Journal of neuroscience : the official journal of the Society for Neuroscience 34, 3130-3141 (2014).
53. A. Goldstein, V. E. Ghazarossian, Immunoreactive dynorphin in pituitary and brain. Proceedings of the National Academy of Sciences of the United States of America 77, 6207-6210 (1980).
54. B. T. Andrews, T. K. McIntosh, M. F. Gonzales, P. R. Weinstein, A. I. Faden, Levels of endogenous opioids and effects of an opiate antagonist during regional cerebral ischemia in rats. J Pharmacol Exp Ther 247, 1248-1254 (1988).
55. B. Cristofori-Armstrong, N. J. Saez, I. R. Chassagnon, G. F. King, L. D. Rash, The modulation of acid-sensing ion channel 1 by PcTx1 is pH-, subtype- and species-dependent: Importance of interactions at the channel subunit interface and potential for engineering selective analogues. Biochem Pharmacol 163, 381-390 (2019).
56. T. Lynagh et al., A selectivity filter at the intracellular end of the acid-sensing ion channel pore. eLife 6 (2017).
57. W. H. Schmied, S. J. Elsasser, C. Uttamapinant, J. W. Chin, Efficient multisite unnatural amino acid incorporation in mammalian cells via optimized pyrrolysyl tRNA synthetase/tRNA expression and engineered eRF1. Journal of the American Chemical Society 136, 15577-15583 (2014).

58. T. Kalstrup, R. Blunck, Reinitiation at non-canonical start codons leads to leak expression when incorporating unnatural amino acids. Scientific reports 5, 11866 (2015).
59. D. S. Dahan et al., A fluorophore attached to nicotinic acetylcholine receptor beta M2 detects productive binding of agonist to the alpha delta site. Proceedings of the National Academy of Sciences of the United States of America 101, 10195-10200 (2004).
60. C. Jin et al., Over-expression of ASIC1a promotes proliferation via activation of the beta-catenin/LEF-TCF axis and is associated with disease outcome in liver cancer. Oncotarget 8, 25977-25988 (2017).
61. K. J. Jensen, P. T. Shelton, S. L. Pedersen, Peptide Synthesis and Applications. J. M. Walker, Ed., Methods in Molecular Biology (Humana Press, Totowa, NJ, Springer Protocols, ed. Second Edition, 2013), vol. 1047.
62. M. Gude, J. Ryf, P. D. White, An accurate method for the quantitation of Fmoc-derivatized solid phase supports. Letters in Peptide Science 9, 203-206 (2002).

Supplementary Information

Supplementary Figures 1-7

Supplementary Tables 1-8

Supplementary Figures

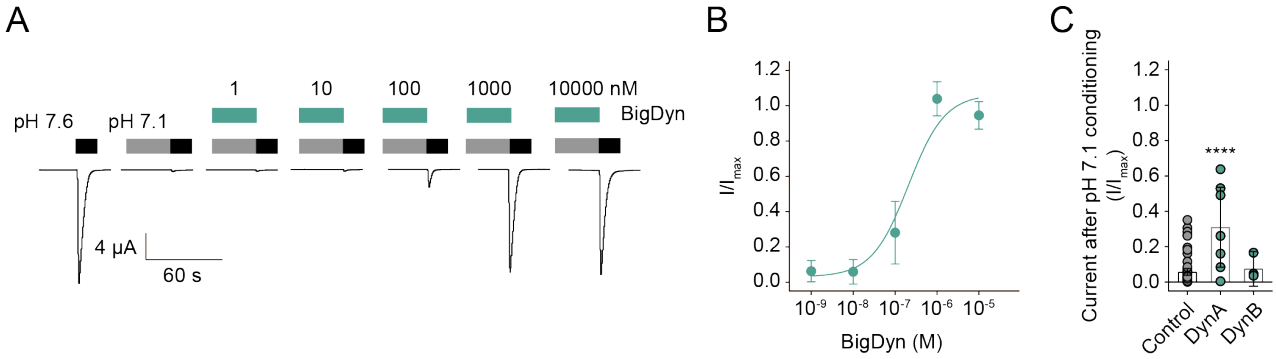

Figure S1: Modulation of ASIC1a by BigDyn, DynA and DynB. (A/B) Representative current traces (A) and normalized data (B) obtained by pH 5.6 application (black bar in (A)) at ASIC1a WT-expressing *Xenopus laevis* oocytes after preincubation in pH 7.1 (grey bar) with or without different concentrations of BigDyn (green bars). EC_{50} of BigDyn is 210 nM (95CI: 162.6, 258.6 nM); in (A) pH 5.6 current response after pH 7.6 incubation is shown as control; data shown as mean ± 95CI; n = 9. (C) Averaged data obtained by pH 5.6 application at mASIC1a WT after preincubation in pH 7.1 (grey bar) with or without the indicated peptide (green bar); each dot represents an individual oocyte and bars represent mean + 95CI. Asterisk in (C) indicates significant difference to control condition (p = 0.0001) n = 4-68.

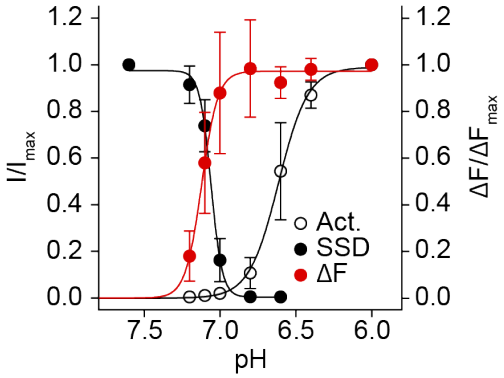

Figure S2: Proton dependence of current and fluorescence signals generated by the Alexa 488-labelled K105C mutant. Normalized current activation and SSD (black traces, left y-axis) and fluorescence (red trace, right Y-axis) signals are plotted as a function of pH. For ΔF the fitting was constrained using min. = 0. Data shown as mean ± 95CI; n = 5.

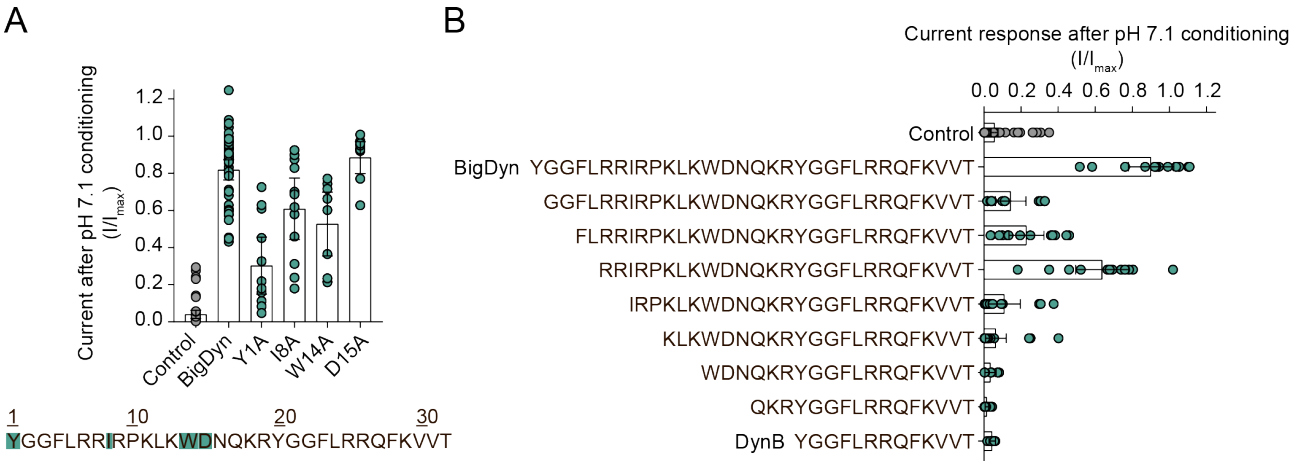

Figure S3: Modulation of ASIC1a by BigDyn derivatives. (A) Averaged data obtained by pH 5.6 application at mASIC1a WT-expressing *Xenopus laevis* oocytes after preincubation in pH 7.1 in the presence of the indicted peptide. Each dot represents an individual oocyte and bars represent mean + 95CI, n = 10-48. The BigDyn sequence with side chains mutated to alanine highlighted in green is shown below the graph. (B) Averaged data obtained for different N-terminal truncation variants of BigDyn obtained by plotting pH 5.6-induced current amplitude after preincubation on pH 7.1 at ASIC1a WT in the presence of the indicated peptide. Each dot represents an individual oocyte and bars represent mean + 95CI; n = 6-68.

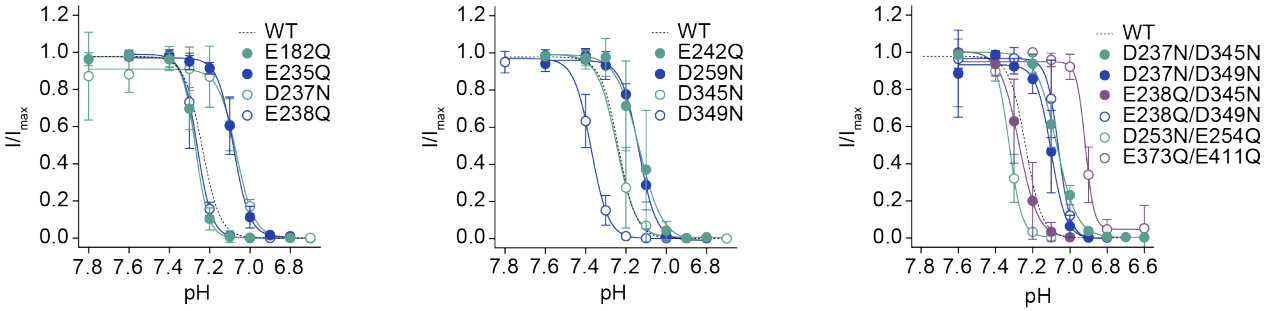

Figure S4: Steady-state desensitization of single and double charge-neutralizing ASIC1a mutants. Normalized SSD plotted versus pH. Data shown as mean ± 95CI; n = 3-64. See Table S6 for further details.

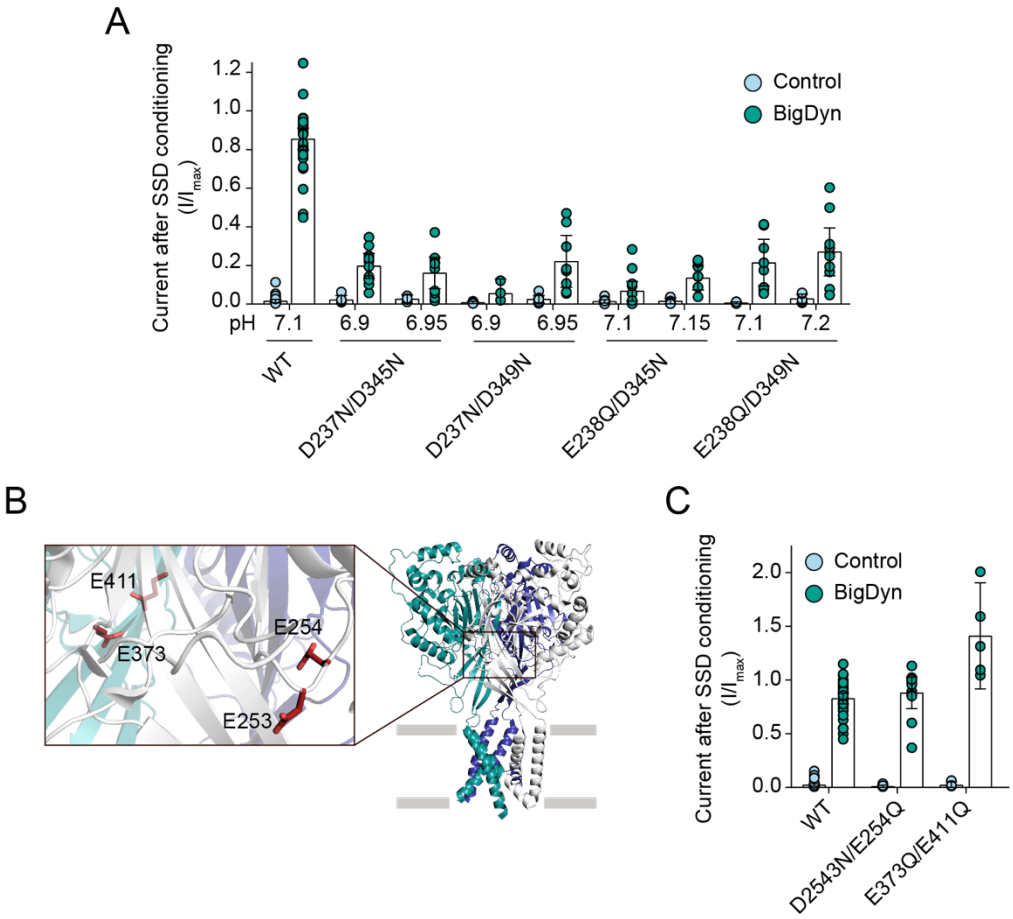

Figure S5: Effects of BigDyn on double-charge neutralizing mutations. (A) Averaged data obtained by pH 5.6 application after preincubation in different SSD-inducing pH conditions with or without BigDyn at *Xenopus laevis* oocytes expressing the indicated double mutant ASIC1a construct. Each dot represents an individual oocyte and bars represent mean + 95CI; n = 4-33. (B) Structure of cASIC1a (PDB: 4NTW) with individual subunits color coded and inset showing the location of acidic side chains away from the acidic pocket that have been mutated to glutamine or asparagine. (C) Averaged data obtained by pH 5.6 (WT and D253N/E254Q) or 4.0 (E373Q/E411) application after preincubation in SSD-inducing pH with or without (control) BigDyn at *Xenopus laevis* oocytes expressing the indicated double mutant ASIC1a construct. Each dot represents an individual oocyte and bars represent mean + 95CI; n = 5-45.

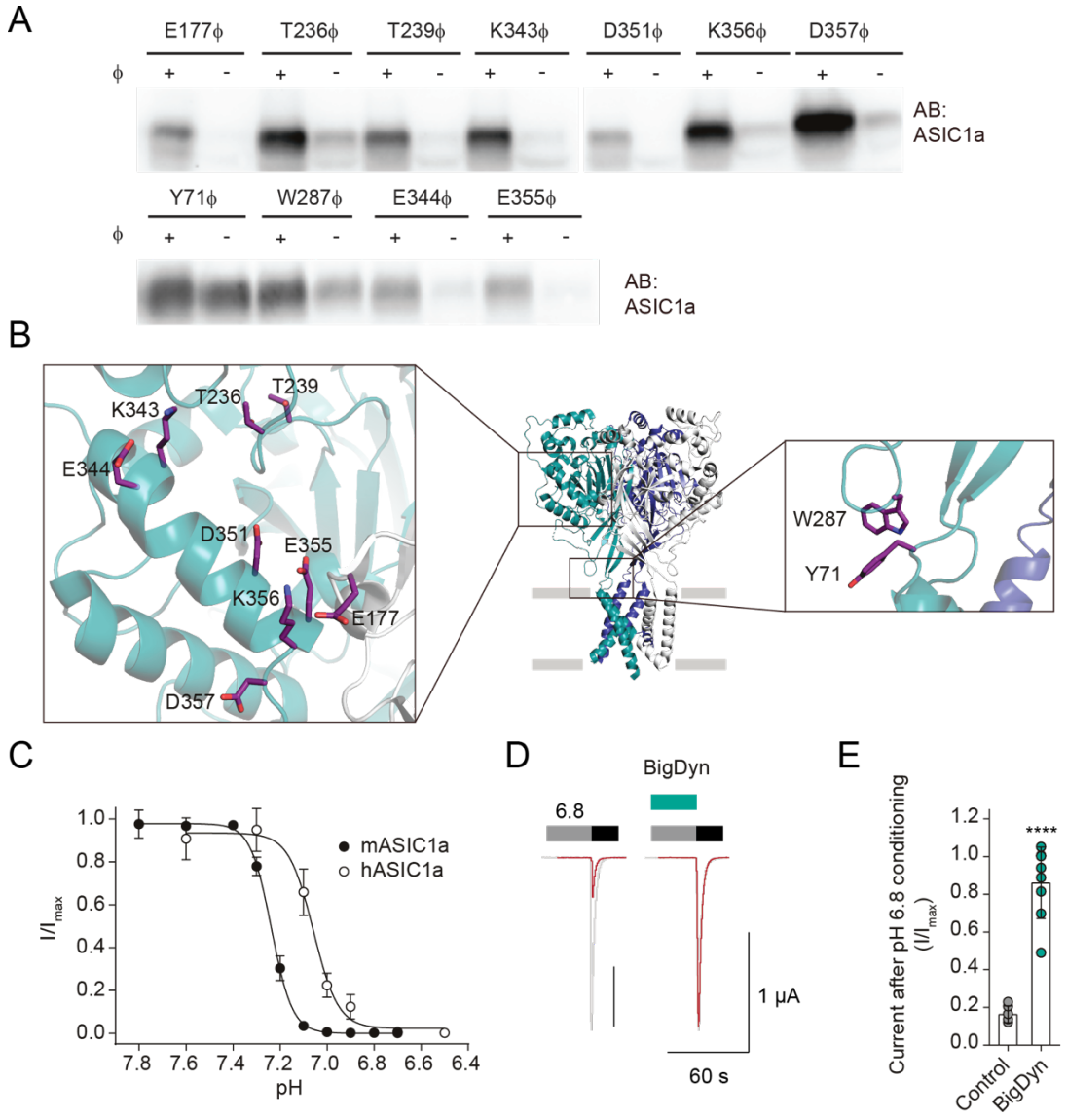

Figure S6: Incorporation of AzF (ϕ) and BigDyn modulation of hASIC1a. (A) Western blot analysis of the indicated stop-codon containing mutants grown in the presence or absence of 0.5 mM ϕ in HEK293 cells. After 48 hrs, the resulting full-length protein was purified via a C-terminal 1D4-tag and visualized by western blotting. With the exception of position 71, all positions tested here showed only small amounts of full length protein in absence of ϕ (compared to those obtained in the presence of ϕ), demonstrating efficient incorporation. (B) Structure of cASIC1a (PDB: 4NTW) with individual subunits color coded and inset highlighting side chains replaced by ϕ in the acidic pocket (left inset) and lower extracellular domain (right inset). (C) SSD of hASIC1a (open, pH_{50} SSD 7.07 (95CI: 7.03, 7.11)) is shifted

compared to mASIC1a (filled, pH_{50} SSD 7.24 (95CI: 7.23, 7.25)). (D/E) Representative current traces (D) and averaged data (E) comparing the normalized pH 5.6-gated current (black bar) remaining after conditioning hASIC1a at desensitizing pH 6.8 (grey bar) in presence (green bar) and absence of 1 μM BigDyn. Data in E is shown as mean ± 95CI, n=6-8 oocytes.

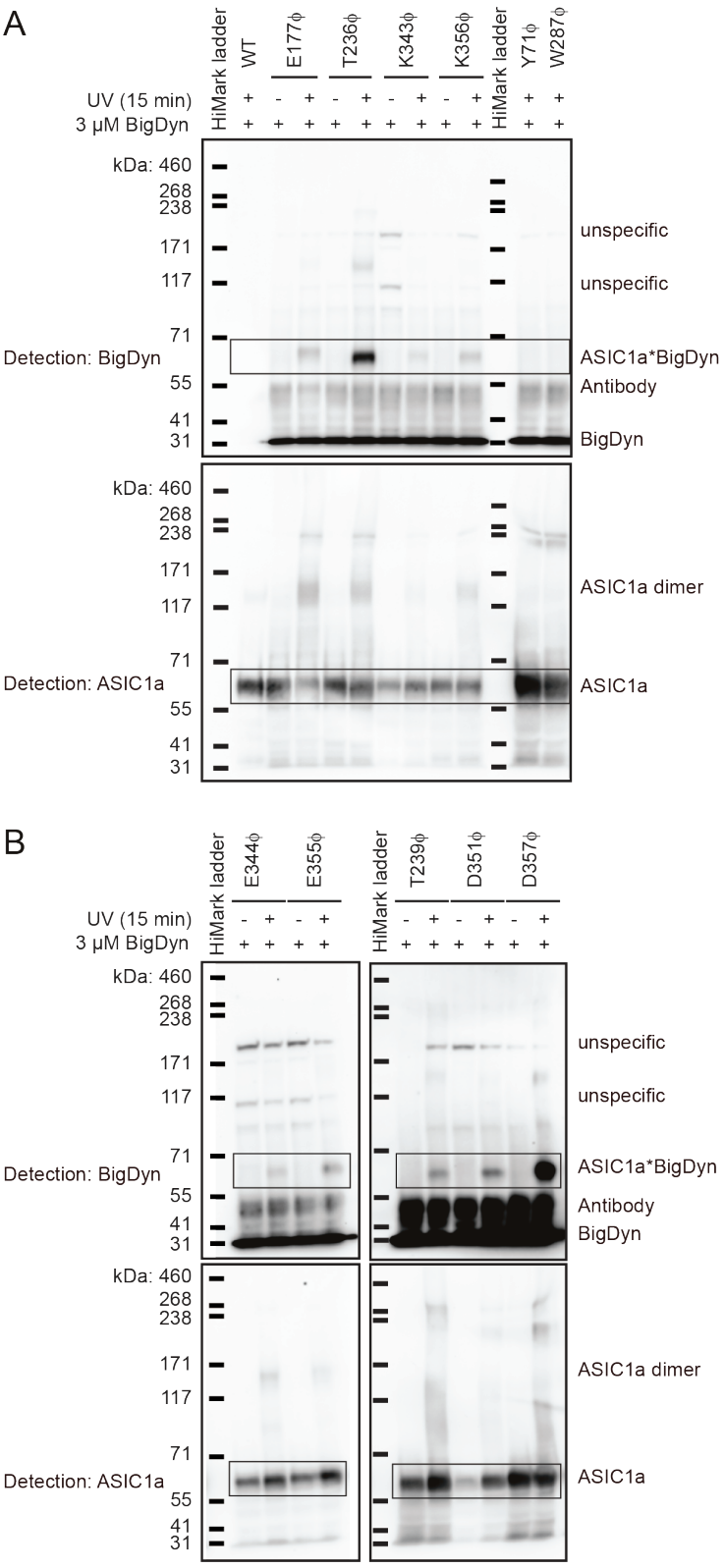

Figure S7: Original Western blots. Areas cropped for Figure 4 are marked with boxes. (A) Western blot for positions 177, 236, 343, 356, 71 and 287. (B) Western blot for positions 344, 355, 239, 351 and 357. Data is representative of two individual experiments.

Table S1: Activation and SSD in absence and presence of BigDyn. pH_{50} and Hill coefficients for activation and steady-state desensitization (SSD) of WT mASIC1a in the absence and presence of 0.1 µM Big Dyn. 95CI stated in parentheses; n = number of experiments; pH_{50}-values and Hill coefficients in presence and absence of BigDyn was compared using an unpaired t-test, asterisks indicate statistically significant differences, n.s = not significant.

		Activation			SSD		
		pH_{50}	Hill coefficient	n	pH_{50}	Hill coefficient	n
0 µM BigDyn	Mean	6.80	5.54	10	7.21	11.74	15
	95CI	(6.70, 6.91)	(2.05, 9.03)		(7.19, 7.24)	(10.12, 13.36)	
0.1 µM BigDyn	Mean	6.66	9.19	8	7.15	9.18	4
	95CI	(6.61, 6.70)	(12.72, 5.66)		(7.12, 7.19)	(3.02, 15.33)	
	p-value	0.0172 *	0.1137 n.s.		0.0225 *	0.1621 n.s.	

Table S2: Peptide and pH-induced fluorescence changes at Alexa Fluor 488-labelled Lys105Cys. Mean fluorescence change (ΔF/F) induced by application of PcTx1 (300 nM), DynB (1 µM), BigDyn (1 µM) or pH 9.0, with 95CI stated in parentheses; n = number of experiments.

	ΔF	95CI	n
PcTx1	46.05	(20.65, 71.44)	7
DynB	-3.02	(-8.864, 2.82)	7
BigDyn	-76.48	(-94.41, -58.56)	15
pH 9.0	1.42	(-7.06, 9.90)	5

Table S3: pH-induced activation, SSD and ΔF at Alexa Fluor 488-labelled Lys105Cys. pH_{50} and Hill coefficients for activation, steady-state desensitization (SSD) and fluorescence change ($\Delta F/\Delta F_{pH5.5}$), with 95CI stated in parentheses; n = number of experiments.

	pH_{50}	95CI	Hill coefficient	95CI	n
Activation	6.61	(6.52, 6.70)	6.02	(7.30, 4.74)	5
SSD	7.06	(7.03, 7.09)	12.10	(11.10, 13.10)	5
ΔF	7.11	(7.06, 7.20)	8.49	(12.24, 4.73)	5

Table S4: Effect of alanine-substituted BigDyn analogs. Mean rescue of current after exposure to SSD-inducing pH at WT mASIC1a, with 95CI stated in parentheses; the effect of the peptides compared to control was analyzed using a one-way ANOVA with a Dunnett's multiple comparisons test, *, $p < 0.05$; ** $p < 0.01$; ***, $p < 0.001$; **** $p < 0.0001$; n = number of experiments; n.s = not significant.

	Rescue	95CI	n	p-value	
Control	4.03	(1.81, 6.28)	46	-	
Big Dyn	81.82	(76.39, 87.24)	48	<0.0001	****
Y1A	30.24	(14.90, 45.59)	12	0.0003	***
R6A	9.78	(-2.07, 5.14)	9	0.9989	n.s
R7A	4.97	(1.16, 8.78)	12	0.9999	n.s
I8A	60.84	(44.23, 77.44)	12	<0.0001	****
R9A	2.35	(1.68, 3.01)	11	0.9997	n.s
K11A	29.35	(10.92, 47.77)	9	0.0031	**
K13A	57.56	(41.24, 73.87)	9	<0.0001	****
W14A	52.68	(35.48, 69.87)	10	<0.0001	****
D15A	88.44	(79.83, 97.05)	10	<0.0001	****
K18A	62.97	(38.62, 87.31)	7	<0.0001	****
R19A	42.73	(31.10, 54.36)	10	<0.0001	****
R25A	76.27	(59.00, 93.54)	10	<0.0001	****
R26A	47.86	(20.45, 75.26)	7	<0.0001	****
K29A	63.36	(40.19, 86.52)	8	<0.0001	****

Table S5: Effect of different dynorphins and truncated BigDyn analogs on mASIC1a SSD. Mean rescue of current after exposure to SSD-inducing pH at WT mASIC1a, with 95CI stated in parentheses; the effect of the peptides compared to control was analyzed using a one-way ANOVA with a Dunnett's multiple comparisons test, *, $p < 0.05$; ** $p < 0.01$; ***, $p < 0.001$; **** $p < 0.0001$; n.s = not significant. n = number of experiments.

Concentration	Peptide	Rescue	95CI	n	p-value	
1 µM	Control	5.73	(3.83, 7.63)	68	-	
	BigDyn	90.11	(77.92, 102.30)	12	<0.0001	****
	DynA	8.36	(5.49, 11.22)	6	0.9995	n.s.
	DynB	4.45	(2.72, 6.19)	6	0.9998	n.s.
	DynA + DynB	5.57	(2.14, 8.99)	5	>0.9999	n.s.
	Dyn(1-19) + DynB	12.83	(1.68, 23.98)	6	0.9228	n.s.
	Dyn(2-32)	14.46	(6.25, 22.68)	12	0.2669	n.s.
	Dyn(4-32)	22.90	(13.44, 32.37)	13	<0.0001	****
	Dyn(6-32)	63.80	(49.46, 78.14)	12	<0.0001	****
	Dyn(8-32)	11.02	(2.43, 19.62)	12	0.915	n.s.
	Dyn(11-32)	6.41	(0.79, 12.03)	18	0.9998	n.s.
	Dyn(14-32)	3.52	(0.48, 6.55)	7	0.9996	n.s.
	Dyn(17-32)	1.58	(0.68, 2.49)	13	0.9851	n.s.
3 µM	DynA	31.02	(8.45, 53.59)	7	<0.0001	****
	DynB	7.49	(-2.27, 17.26)	4	0.9997	n.s.

Table S6: Characterization pH dependence of SSD of WT and mutant mASIC1a and WT hASIC1a. pH_{50} and Hill coefficients for steady-state desensitization (obtained with indicated activating pH), including resulting pH to induce SSD (SSD pH). 95CI stated in parentheses; n = number of experiments, E373Q/E411Q was characterized on a single batch of oocytes.

	SSD pH_{50}	95CI	Hill coefficient	95CI	n	Activation pH	SSD pH
WT	7.24	(7.23, 7.25)	12.61	(11.82, 13.40)	64	5.6	7.1
E182Q	7.27	(7.25, 7.29)	14.04	(12.83, 15.25)	8	5.6	7.1
E235Q	7.08	(7.06, 7.11)	12.39	(11.40, 13.38)	8	5.6	6.9
D237N	7.07	(7.05, 7.10)	12.31	(9.13, 15.49)	8	5.6	6.9
E238Q	7.26	(7.24, 7.28)	13.87	(8.87, 18.87)	7	5.6	7.1
E242Q	7.14	(7.07, 7.21)	11.57	(8.51, 14.63)	6	5.6	6.9
D259N	7.14	(7.13, 7.15)	10.46	(8.19, 12.73)	6	5.6	7.0
D345N	7.24	(7.19, 7.29)	12.64	(10.13, 15.15)	9	5.6	7.1
D349N	7.38	(7.35, 7.40)	12.54	(9.81, 15.28)	11	5.6	7.2
D237N/D345N	7.06	(7.04, 7.08)	10.23	(7.97, 12.49)	14	4	6.9
D237N/D349N	7.10	(7.07, 7.13)	12.67	(9.64, 15.70)	5	5.6	6.95
E238Q/D345N	7.27	(7.22, 7.32)	9.61	(9.00, 10.22)	5	5.6	7.1
E238Q/D349N	7.33	(7.31, 7.34)	13.63	(11.75, 15.50)	8	5.6	7.2
D253N/E254Q	7.06	(7.03, 7.09)	15.93	(13.09, 18.76)	6	5.6	6.9
E373Q/E411Q	6.92	(6.90, 6.93)	19.39	(9.48, 29.31)	3	4	6.8
hASIC1a WT	7.07	(7.03, 7.11)	8.11	(4.61, 11.61)	6	5.6	6.8

Table S7: Effect of 1 μM BigDyn on SSD of single and double mutant mASIC1a. Mean rescue of current after exposure to SSD-inducing pH (SSD pH) at WT and mutant mASIC1a in the absence (Control) and presence of 1 μM BigDyn (BigDyn), with 95CI stated in parentheses; the rescue in presence of BigDyn compared to Control was analyzed using an unpaired t-test, *, $p < 0.05$; ** $p < 0.01$; ***, $p < 0.001$; **** $p < 0.0001$; n.s = not significant; n = number of experiments..

		Control			BigDyn				
	SSD pH	Rescue	95CI	n	Rescue	95CI	n	p-value	
WT	7.1	2.31	(1.26, 3.36)	45	82.81	(77.80, 87.82)	41	<0.0001	****
E182Q	7.1	0.93	(-0.48, 2.33)	7	82.01	(65.55, 98.48)	7	<0.0001	****
E235Q	6.9	3.30	(0.90, 5.63)	4	88.29	(85.35, 91.22)	6	<0.0001	****
D237N	6.9	3.95	(2.07, 5.84)	10	81.16	(68.27, 94.05)	14	<0.0001	****
E238Q	7.1	12.30	(4.87, 19.74)	9	69.74	(50.55, 88.93)	9	<0.0001	****
E242Q	6.9	4.64	(-1.30, 10.57)	6	92.86	(82.27, 103.40)	9	<0.0001	****
D259N	7.0	8.65	(4.20, 13.10)	9	69.59	(56.38, 82.81)	13	<0.0001	****
D345N	7.1	7.69	(2.20, 13.17)	8	58.92	(42.53, 75.31)	10	<0.0001	****
D349N	7.2	2.01	(-1.49, 5.50)	7	49.69	(36.20, 63.19)	12	<0.0001	****
D237N/D345N	6.9	2.24	(0.10, 4.37)	6	19.79	(13.27, 26.32)	10	0.0004	***
	6.95	2.27	(0.56, 4.83)	4	16.08	(7.99, 24.18)	10	0.0400	*
D237N/D349N	6.90	0.84	(0.29, 13.98)	5	5.53	(-2.04, 13.09)	4	0.0609	n.s.
	6.95	2.63	(0.72, 4.53)	7	22.13	(8.77, 35.48)	8	0.0071	**
E238Q/D345N	7.1	1.43	(0.59, 2.27)	10	6.766	(1.69, 11.84)	13	0.0606	n.s.
	7.15	1.65	(0.18, 3.13)	6	13.62	(7.30, 19.94)	8	0.0026	**
E238Q/D349N	7.1	0.70	(0.24, 1.17)	6	21.45	(9.40, 33.51)	8	0.0045	**
	7.2	2.79	(0.39, 5.19)	6	27.03	(14.66, 39.40)	10	0.0046	**
D253N/E254Q	6.9	1.06	(-0.02, 2.13)	7	88.07	(73.45, 102.70)	11	<0.0001	****
E373Q/E411Q	6.8	2.25	(-0.61, 5.11)	5	141.1	(91.66, 190.50)	5	<0.0001	****

Table S8: Synthesized peptides. Listed are peptide name, sequence, purity, as well as calculated and observed mass, respectively.

Peptide	Sequence	Purity (%)	Calc. Mass ($M+H^+$)	Obs. Mass ($M+H^+$)
Big dynorphin	YGGFLRRIRPKLKWDNQKRYGGFLRRQFKVVT	>95	3984.66	3984.45
Dynorphin A	YGGFLRRIRPKLKWDNQ	>95	2147.48	2147.25
Dynorphin B	YGGFLRRQFKVVT	>95	1570.84	1570.90
N-terminal truncations				
Dyn(2-32)	GGFLRRIRPKLKWDNQKRYGGFLRRQFKVVT	>95	3821.49	3821.31
Dyn(4-32)	FLRRIRPKLKWDNQKRYGGFLRRQFKVVT	91	3707.39	3706.80
Dyn(6-32)	RRIRPKLKWDNQKRYGGFLRRQFKVVT	92	3447.06	3446.92
Dyn(8-32)	IRPKLKWDNQKRYGGFLRRQFKVVT	>95	3134.68	3134.36
Dyn(11-32)	KLKWDNQKRYGGFLRRQFKVVT	95	2768.22	2868.04
Dyn(14-32)	WDNQKRYGGFLRRQFKVVT	>95	2398.72	2398.29
Dyn(17-32)	QKRYGGFLRRQFKVVT	87	1983.32	1983.00
Ala-substitution				
Dyn(Y1A)	AGGFLRRIRPKLKWDNQKRYGGFLRRQFKVVT	>95	3892.57	3892.29
Dyn(R6A)	YGGFLARIRPKLKWDNQKRYGGFLRRQFKVVT	>95	3899.55	3898.95
Dyn(R7A)	YGGFLRAIRPKLKWDNQKRYGGFLRRQFKVVT	>95	3899.55	3899.22
Dyn(I8A)	YGGFLRRARPKLKWDNQKRYGGFLRRQFKVVT	>95	3942.58	3941.19
Dyn(R9A)	YGGFLRRIAPKLKWDNQKRYGGFLRRQFKVVT	>95	3899.55	3898.65
Dyn(K11A)	YGGFLRRIRPALKWDNQKRYGGFLRRQFKVVT	93	3927.57	3927.09
Dyn(K13A)	YGGFLRRIRPKLAWDNQKRYGGFLRRQFKVVT	>95	3927.57	3926.86
Dyn(W14A)	YGGFLRRIRPKLKADNQKRYGGFLRRQFKVVT	>95	3869.53	3869.32
Dyn(D15A)	YGGFLRRIRPKLKWANQKRYGGFLRRQFKVVT	>95	3940.08	3940.65
Dyn(K18A)	YGGFLRRIRPKLKWDNQARYGGFLRRQFKVVT	>95	3927.57	3927.04
Dyn(R19A)	YGGFLRRIRPKLKWDNQKAYGGFLRRQFKVVT	>95	3899.55	3899.28
Dyn(R25A)	YGGFLRRIRPKLKWDNQKRYGGFLARQFKVVT	>95	3899.55	3899.04
Dyn(R26A)	YGGFLRRIRPKLKWDNQKRYGGFLRAQFKVVT	>95	3899.55	3899.24
Dyn(K29A)	YGGFLRRIRPKLKWDNQKRYGGFLRRQFAVVT	>95	3927.57	3926.64